Article

Support Vector Machine-Based Soft Decision for Consecutive-Symbol-Expanded 4-Dimensional Constellation in Underwater Visible Light Communication System

Wenqing Niu [1], Jifan Cai [1], Zhiteng Luo [1], Jianyang Shi [1] and Nan Chi [1,2,3,*]

[1] Key Laboratory for Information Science of Electromagnetic Waves (MoE), Department of Communication Science and Engineering, Fudan University, Shanghai 200433, China

[2] Shanghai Engineering Research Center of Low-Earth-Orbit Satellite Communication and Applications, Shanghai 200433, China

[3] Shanghai Collaborative Innovation Center of Low-Earth-Orbit Satellite Communication Technology, Shanghai 200433, China

[*] Correspondence: nanchi@fudan.edu.cn

Abstract: Nowadays, underwater visible light communication (UVLC) has become one of the key technologies for high-speed underwater wireless communication. Because of the limited modulation bandwidth and nonlinearity of the optoelectronic devices in the UVLC system, the combination of inter-symbol interference and nonlinear impairment will inevitably degrade the transmission performance. Advanced digital signal processing methods including equalization and decoding are required. In the past few years, Support vector machine (SVM) has been widely investigated in quadrature amplitude modulation (QAM) for soft decision in the decoding process. However, previous works only consider 2-dimensional (2-D) separate symbol, ignoring the correlation between consecutive symbols. In this paper, we propose to use SVM for soft decision with a 4-dimensional (4-D) constellation by concatenating two consecutive symbols. To deal with the increasing computational complexity in the SVM training phase, bit-based binary SVM multi-class strategy and an edge-detection-based data pre-processing method are employed. In this paper, we demonstrate a carrierless amplitude and phase (CAP) 16-QAM UVLC system. Experimental results indicate that the performance is greatly improved when using consecutive-symbol-expanded 4-D constellation with SVM for soft decision.

Keywords: underwater visible light communication (UVLC); support vector machine (SVM); inter-symbol interference

1. Introduction

With the development of ocean exploration, the demand for high-speed underwater wireless data transmission is increasing. Since radio frequency is not suitable for underwater communication because of the great power attenuation [1], acoustic communication is widely used, but due to the low transmission speed and large latency, the typical data rate of acoustic communication is extremely limited. Due to the low attenuation window [2,3] at blue-green spectrum, underwater visible light communication (UVLC) is supposed to provide long-distance and high-speed transmission, and abundant investigations on light-emitting diodes (LEDs) have been reported [1,4–7].

However, inter-symbol interference (ISI) and nonlinear impairment are the two main problems that restrict the performance of UVLC system. On the one hand, the UVLC system is bandwidth-limited due to the low modulation bandwidth of LED [5], and the low-pass filtering effect will induce severe ISI. On the other hand, the UVLC channel is faced with absorption, scattering, and turbulence [8]. Therefore, large driving power is required to ensure the desired signal-to-noise ratio (SNR) at the receiver. The nonlinearity

from optoelectronic devices such as LEDs, photodiodes, and electrical amplifiers (EAs) [6,7] becomes severe at high amplitude.

In order to eliminate the combination of ISI and nonlinear impairment, digital signal processing (DSP) is required. Generally, DSP includes equalization and decoding. Constant modulo algorithm (CMA), least mean square (LMS)-based linear equalizers, and Volterra series or polynomial-based nonlinear equalizers [9–11] have been widely investigated. As to decoding, hard decision based on Euclidean distance is most commonly used, whereas soft decision is supposed to provide better performance. In this context, the latest researches have employed machine learning algorithms such as support vector machine (SVM) [12–15] and K-means [16,17] for soft decision. SVM-based soft decision is especially effective for quadrature amplitude modulation (QAM) when there is strong nonlinearity [14,15], because the decision boundary can be adjusted according to the distribution characteristics of constellation points. However, previous works mainly concentrate on 2-dimensional (2-D) separate symbol [12–15], whereas the correlation between consecutive symbols is ignored. Inspired by [18,19], the constellation can be expanded to a higher dimensional constellation by concatenating consecutive symbols. For QAM signal, the original 2-D constellation is expanded to a 4-D constellation. The nonlinear effect and ISI interact with each other. It is difficult to remove the correlation between adjacent symbols thoroughly with a feedforward equalizer, and the high-dimensional clusters will be distorted due to the combination of residual ISI and nonlinear impairment.

In this paper, we propose to employ SVM to find the optimal decision hyperplane for the consecutive-symbol-expanded 4-D constellation in an experimental UVLC system. The proposed scheme is used for soft decision, independent of the post-equalization process. As the intensity modulation-direct detection (IM-DD) system requires a real and positive signal, a pair of carrierless amplitude and phase (CAP) shaping filters are used for CAP modulation [20,21] so that the complex-valued QAM signal can be converted into a real-valued signal. Different from existing works that employ SVM for 2-D normal constellation [12–15], the correlation between consecutive symbols is considered in this work. However, for the consecutive-symbol-expanded 4-D constellation, the computational complexity of SVM training phase becomes higher because of the demand for more classifiers and larger training data size. To deal with the high computational complexity resulting from the demand for more classifiers, the bit-based binary SVM is applied as the multi-class SVM strategy, so that the number of required classifiers can remain small [15]. Additionally, since a SVM model only depends on a few support vectors [12], which are the nearest to the hyperplane, it can be more efficient if the edge points are picked out in advance because the support vectors are included in the edge points. To deal with the high computational complexity resulting from the demand for larger training data size, a simple data pre-processing method is used during the SVM training phase to detect the edge points of each cluster and abandon the redundant training data. Experimental results prove the feasibility of the proposed method. When LMS-based linear equalizer is used for post-equalization, the available baud rate is increased to 412.5 MBaud with the proposed method under the 7% forward error correction (FEC) threshold.

2. Principle

2.1. Concept of Support Vector Machine

SVM is a powerful supervised machine learning algorithm which can be applied for amplitude and phase noise characterization [22]. SVM-based soft decision for QAM and APSK constellation has been proposed in optical communication system, and shown great improvement especially when there is strong nonlinearity. Because traditional hard decision is based on the Euclidean distance of separate symbol, it only works well when the noise distribution follows independent identical distribution for all levels. SVM, on the other hand, can provide accurate classification boundary according to the characteristics of noise distribution through training data set. Therefore, SVM-based soft decision is superior to Euclidean distance-based hard decision.

In general, the in-phase and quadrature (I/Q) components are concatenated as 2-D feature vectors. If the training data set is not linearly separable, the kernel function can be used to map the data from the lower-dimensional feature space to a higher-dimensional feature space [12], so that the data can be linearly separated. According to the statistical learning theory, the main function of SVM is to find an optimal hyperplane that ensures the minimum distance from the optimal hyperplane to the nearest points of each group is maximum, namely the maximizing margin rule [14,23]. Given the function of the hyperplane,

$$\mathbf{w}^T \cdot \mathbf{x} - b = 0, \tag{1}$$

where $\mathbf{x}$ is the feature vector, and $\mathbf{w}$ and b denote the weight and bias. Equation (2) describes the max-margin problem [23]:

$$\begin{aligned} \min_{\{\mathbf{w},b\}} \quad & \tfrac{1}{2}\|\mathbf{w}\| + C\sum_{i=1}^{n} \xi_i \\ \text{s. t.} \quad & \mathbf{y}_i(\mathbf{w}^T \cdot \mathbf{x}_i - b) \geq 1 - \xi_i \end{aligned} \tag{2}$$

where $2/\|\mathbf{w}\|$ is the margin, and $\mathbf{y}i \in \{\pm 1\}$ denoting the binary class of $\mathbf{x}_i$. The penalty parameter C and the non-negative slack variable ξ_i are introduced to provide a soft margin [23]. C is also related to the box constraint, which controls the penalty imposed on margin-violating observations [24]. A small box constraint provides a more flexible model that can prevent overfitting. The points closest to the hyperplane are named support vectors. In other words, the trained optimal hyperplane only depends on a few support vectors.

As SVM is originally proposed for binary classification, for data set with more than two classes, additional multi-class SVM strategy is required to decompose the multi-class problem into several binary classifiers. Common multi-class strategies include one-versus-one (OVO), one-versus-rest (OVR), and directed acyclic graph (DAG) [13]. The number of required classifiers for different multi-class strategies is displayed in Table 1. For m-QAM constellation, bit-based binary classifiers [13–15] can achieve excellent performance with only $\log_2 m$ classifiers. The bit-based binary SVM is effective for m-QAM signal with an even $\log_2 m$, because the constellation points are evenly distributed in a lattice and the bit-to-symbol mapping follows gray coding, the adjacent symbols have one single bit differing. Intuitive bit-based classification hyperplanes can be easily obtained.

Table 1. The number of required classifiers for different multi-class strategy.

Multi-Class Strategy	Number of Classifiers
OVO SVM	$m(m-1)/2$
OVR SVM	m
Bit-based binary SVM	$\log_2 m$

2.2. SVM-Based Soft Decision for 4-D Constellation

Given the transmitting m-QAM sequence $s(n)$ and the receiving sequence $r(n)$, previous works about SVM-based soft decision only consider the separate symbol $(r_I(n), r_Q(n))$ as the 2-D feature vector (x_1, x_2), whereas the correlation between consecutive symbols is ignored. By concatenating the I/Q components of two consecutive symbols, the original 2-D constellation is expanded to the 4-D constellation. Generally, considering more consecutive symbols may provide better performance, the additional computational complexity should also be considered. For the m-order QAM signal, the combinations of consecutive symbols will increase to m^n with n-consecutive-symbol-expanded high-dimensional constellation. The complexity grows rapidly as the number of consecutive symbols increases. However, strong interference usually comes from adjacent symbols, and most of the ISI can be eliminated by the equalization process. Therefore, we mainly consider 2-consecutive-symbol-expanded 4-D constellation for soft decoding. The 4-D feature vector (x_1, x_2, x_3, x_4) for SVM is $(r_I(n), r_Q(n), r_I(n+1), r_Q(n+1))$. The $2m$-bit binary labels of the 4-D feature vectors

are generated by concatenating the original *m*-bit binary labels of the two consecutive labels, so that we can ensure that if the bit-to-symbol mapping of the original 2-D constellation follows gray coding, the bit-to-symbol mapping of the expanded 4-D constellation also follows gray coding. Thus, the proposed scheme can be employed for *m*-order QAM signal with an even $\log_2 m$. The combinations of consecutive symbols for 64-QAM are 64^2, the required training data size is too large for implementation, while the spectral efficiency QPSK seems not sufficient for a high-speed UVLC system. As a result, we choose 16-QAM for validation. As Figure 1a shows, we decompose the 4-D constellation into four 3D diagrams according to the $s_Q(n + 1)$ level. Different colors denote different labels. There are 256 (16^2) labels, corresponding to the 8-bit binary sequence.
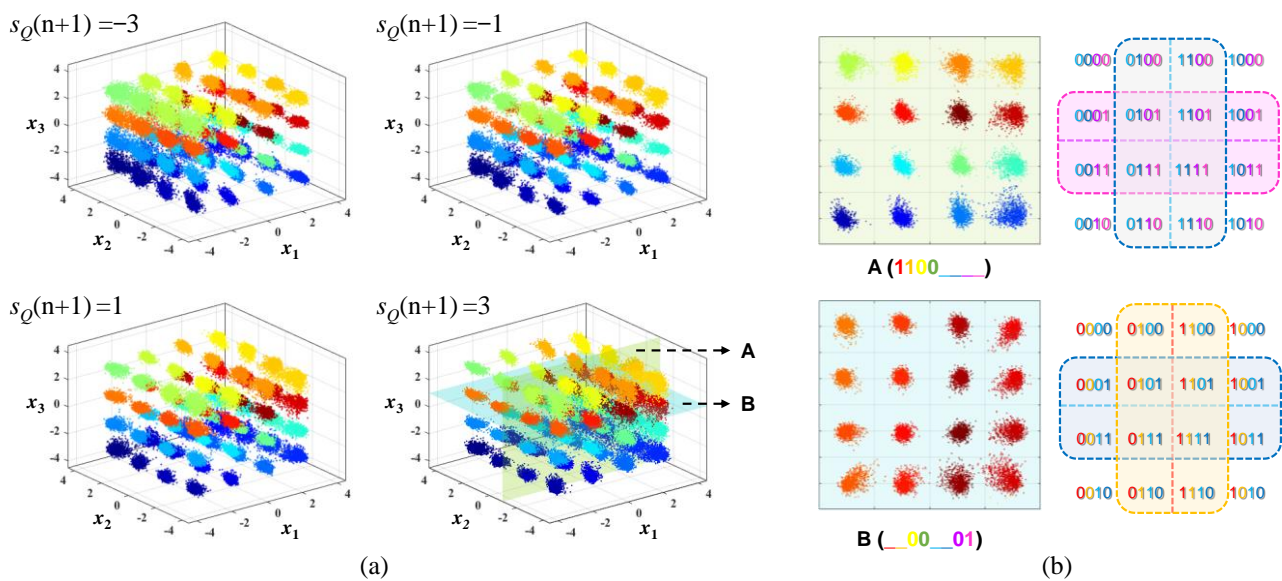

Figure 1. (**a**) Constellation diagrams of two consecutive symbols in simulated limited nonlinear channel. (**b**) Bit-based binary multi-class SVM strategy.

As for the multi-class SVM strategy, the common OVO and OVR methods are not suitable for the expanded high-dimensional constellation anymore, because the number of classes increases from 16 to 256. The numbers of required classifiers for OVO and OVR become 32,640 and 256, respectively, whereas the number of required classifiers for the bit-based binary SVM is $\log_2 m$. If bit-based binary SVM is employed as the multi-class strategy, only 8 classifiers are needed, corresponding to the binary label of the 4-D constellation. Therefore, the complexity can be significantly reduced.

Furthermore, in order to go through enough points in each class, a large amount of training data is needed. However, as mentioned above, the SVM classification hyperplane only depends on a few support vectors. There are redundant training data which have no contribution to the SVM training phase but instead bring high computational complexity. It can be more efficient if the edge points are picked out in advance. As the support vectors are the closest to the hyperplane, we can infer that these support vectors are included in the edge points of each training data cluster. Therefore, we propose to use a data preprocessing method to reduce the redundant training data. As Figure 2a shows, the 4-D training feature vectors (x_1, x_2, x_3, x_4) can be decomposed to six 2-D constellations. It is noted that the I/Q scale of the constellation is ranging from [−4, 4]. Then, the constellations are converted to six binary images through pixel division. The pixel size is denoted as Rs. The number of pixels is $(4/Rs)^2$. Next, the Sobel operator, which performs a 2-D spatial gradient measurement, is used for edge detection, so that only the points in the edge pixel are picked out and merge to the new training feature vectors (x'_1, x'_2, x'_3, x'_4). Then, the bit-based binary SVM classifiers are established based on the pre-processed training data set. At the

testing phase, each binary SVM classifier gives a predicted answer (0 or 1). Finally, the 8-bit label can be converted to the decimal label.
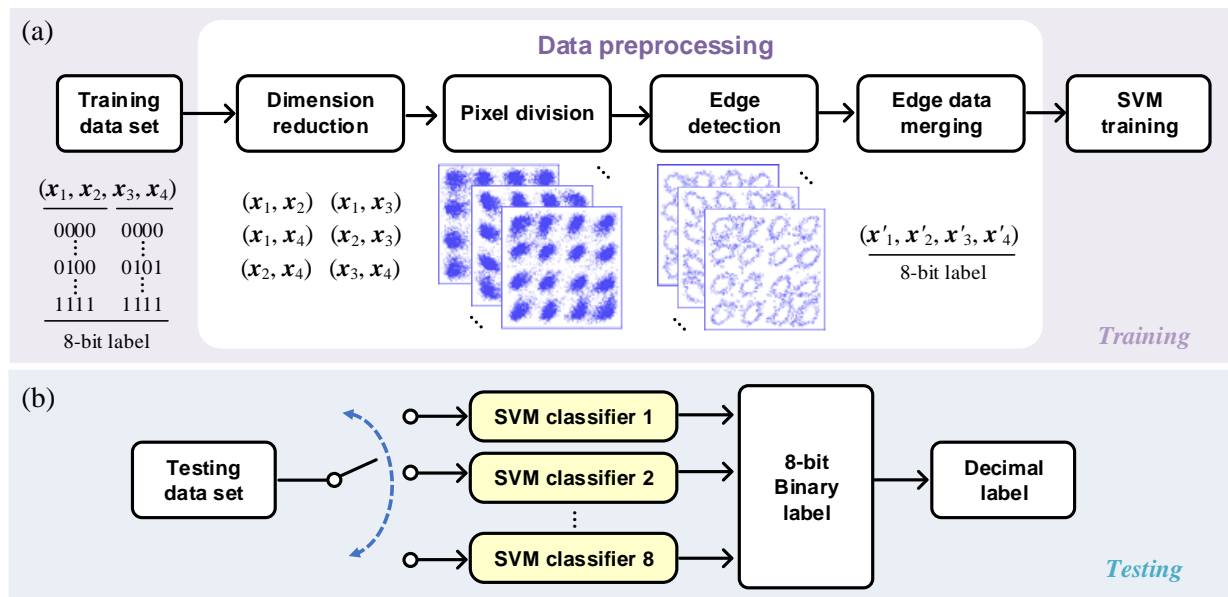
Figure 2. Schematic of SVM-based soft decision. (**a**) SVM training phase with data preprocessing. (**b**) SVM testing phase.

3. Experimental Setup

Figure 3 shows the experimental setup for the underwater visible light communication system. The original binary data are generated from an offline MATLAB program. First, the binary data are mapped into 16-QAM symbols. After a 4-time up-sampling, the in-phase and quadrature parts of the complex-valued QAM symbols are separated. Then, a pair of orthogonal shaping filters (roll-off factor = 0.205) are used for CAP modulation. Afterward, the real-valued signal is loaded into an arbitrary waveform generator (Tektronix AWG710B, 4.2GSa/s). As the typical −3 dB modulation bandwidth of large-scale LED is limited to a dozen of MHz or lower, a hardware pre-equalization circuit is used to increase the power of high-frequency component and decrease the power of low-frequency component [20]. The hardware pre-equalization circuit is a single constant-resistance symmetrical bridged-T amplitude equalizer [20] with the resonant frequency at 500 MHz and low-frequency attenuation 28dB. Afterward, the signal is sent to an amplifier (ZHL-2-8-S+), followed by a Bias Tee (ZFBT-4R2GW-FT+) which couples the signal and direct current to drive a blue LED (−3 dB bandwidth is 17 MHz) [7]. After transmission through a 1.2 m water tank, the signal is focused by a lens (Ø75 mm, f = 60 mm) and detected by a PIN (Hamamatsu, S10784). Tap water is used in this experiment. The system is line-of-sight point-to-point transmission and turbulence can be ignored, so that the UVLC channel is approximately deterministic. The PIN outputs two opposite signals which are subtracted after the amplifier, oscilloscope (DSO9404A, 20GSa/s) and synchronization to suppress the common mode noise of the system.

Then, the received signal is sent into the offline digital signal processing (DSP) block for data recovery. First, two matched filters are employed for CAP demodulation. Since the zero-forcing (ZF) pre-equalization to obtain a flat spectrum is not suitable in UVLC system [25], the hardware pre-equalization circuit merely provides the rough power allocation and a more balanced SNR distribution. After down-sampling, LMS-based linear adaptive post-equalization is used to mitigate the ISI. The tap-number of the LMS-based linear equalizer is 21, and the step-size is optimized at every operating condition in this experiment. Next, the proposed SVM-based soft decision for 4-D constellation is used to determine the 4-D decision boundary. We use radial basis function (RBF) as the kernel

function. The detail implementation about the scheme has been introduced in Section 2.2. Finally, the original data are recovered after QAM de-mapping.
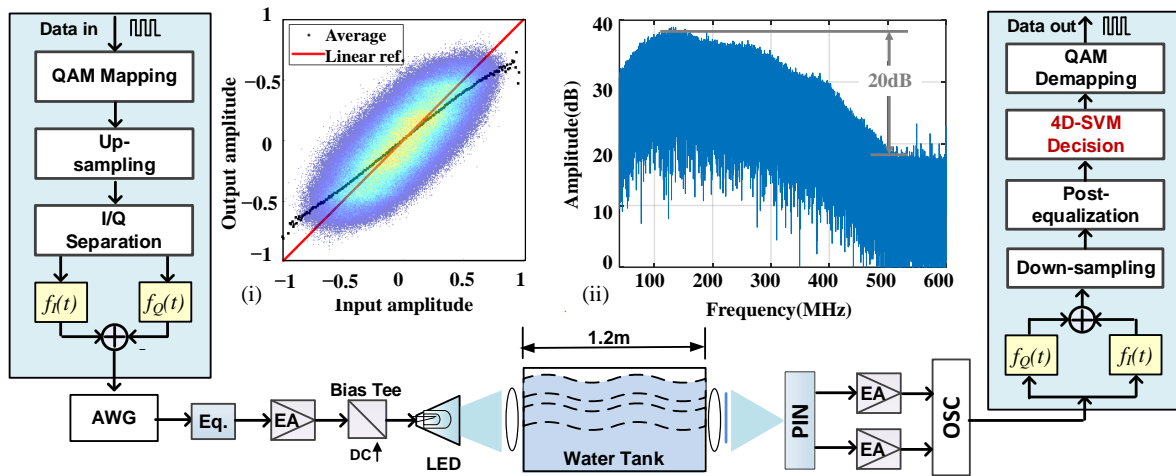

Figure 3. Experimental setup of the underwater visible light communication system.

The inset (i) shows the normalized input amplitude–output amplitude (AM–AM) of the UVLC system at 1.1V and 1.6 Gbps. The red line is the linear reference. The black points are the average value in a small grid of input amplitude. Obviously, the AM–AM curve displays nonlinear effect. The inset (ii) is the spectrum of the received signal which is obtained by fast Fourier transform (FFT). The baud rate of the signal is 400 MBaud. Although hardware pre-equalization circuit is applied, the high frequency component still displays great attenuation. In summary, the system is working at nonlinear and bandwidth-limited condition. It is difficult to remove the correlation between adjacent symbols thoroughly. Independent of the equalization method, the proposed method is used for soft decision, which enhances the decoder.

4. Results and Discussion

This section introduces the experimental results and discussion. First, the performance of SVM-based soft decision for normal 2-D constellation and consecutive-symbol-expanded 4-D constellation at different training data size is given in Figure 4. It should be noted that the system is working at 1.1 V and 1.6 Gbps, and data preprocessing is not employed. As Figure 4a shows, the convergence speed for normal constellation with SVM is faster because the number of classes is smaller, whereas, if there are enough training data, 4-D constellation with SVM can provide better bit error rate (BER) performance. However, as Figure 4b shows, the percentage of support vector (SV) in the training data is decreasing when there is more training data. It indicates that there are considerable redundant training data. The complexity of the training phase scales between $O(dN_t^2)$ and $O(dN_t^3)$ for SVM with d-dimensional feature vectors and N_t training points. Therefore, data preprocessing is necessary for reducing computational complexity. To make a trade-off between BER performance and SVM training complexity, the training data size is set as 26,214. The trained SVM models can be applied for a period of time, because the system is approximately deterministic at a fixed operating condition. In a practical system, the training process can be operated offline for some typical operating conditions.

(a)

(b)
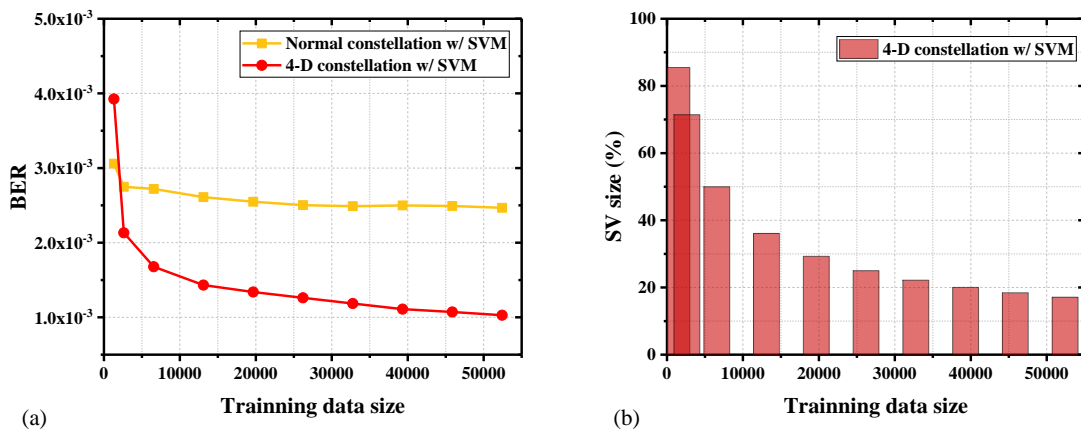
Figure 4. (**a**) BER versus training data size. (**b**) The percentage of SV size versus training data size for 4-D constellation with SVM.

To search for the optimal parameters for the data preprocessing method, we measure the BER performance and the compression ratio (N_{edge}/N) with different pixel size Rs and Threshold of the Sobel operator. First, the experimental results are measured at a data rate of 1.6 Gbps and V_{pp} of 1.1 V, as shown in Figure 5a,b. Figure 5a shows the BER performance under different parameter conditions. The area with larger value indicates a better BER performance. However, not all the Threshold and Rs pairs with large-log (BER) are appropriate to simplify the training data set in the edge detection process. Figure 5b shows the compression ratio of the training data after pre-processing. The area with a lower value indicates that the Sobel edge detector worked and the training set becomes simplified, to a certain extent. To make a tradeoff between the BER performance and compression ratio, we prefer the parameters that correspond to lower BER and lower N_{edge}/N. As a result, at the data rate of 1.6 Gbps, the optimal Threshold ranges from 0.1 to 0.23, while the optimal Rs ranges from 0.057 to 0.08. To ensure the generalization of the optimal parameters, the BER performance is also measured at the operating condition of 1.1 V, 1.4 Gbps. The results are shown in Figure 5c,d. Similarly, at the data rate of 1.4 Gbps, the optimal threshold ranges from 0.1 to 0.23, meanwhile the optimal Rs ranges from 0.057 to 0.08. The optimal ranges are coincident with that at the data rate of 1.6 Gbps.

(a)

(b)

(c)

(d)
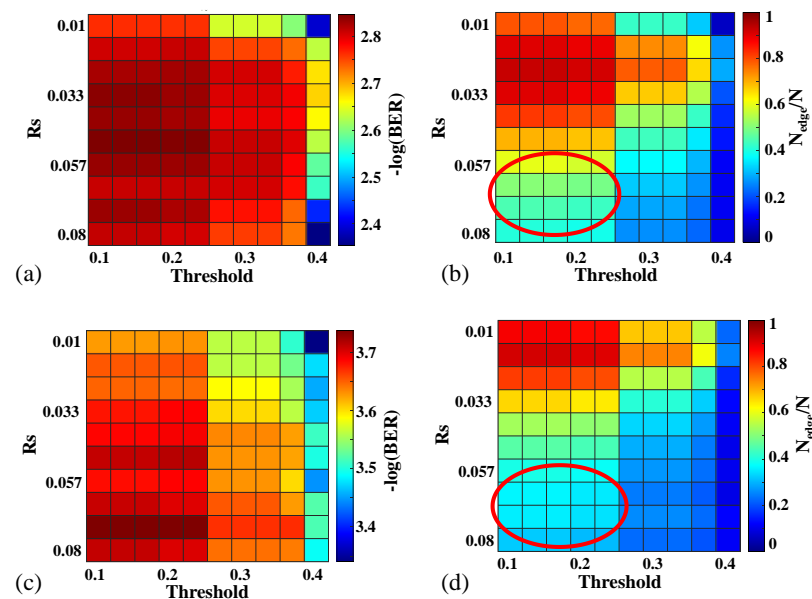
Figure 5. Parameter selection based on grid search. (**a**) BER performance, and (**b**) at 1.6 Gbps. (**c**) BER performance, and (**d**) at 1.4 Gbps.

More specifically, as Figure 6a shows, we illustrate the BER performance versus Rs in the case of two fixed Threshold values under the condition of a data rate of 1.6 Gbps and V_{pp} of 1.1 V. When Threshold equals 0.2, the BER keeps a low value. The constellation diagrams after edge detecting under certain values of Rs are inserted as subfigures. We can observe that the constellation F obtains a clear profile, which effectively reduces the training data size. By contrast, constellation B shows that the edge detection algorithm has not obtained a good result and that there are many redundant data even though BER performance is barely satisfactory. Similarly, as Figure 6b shows, we also illustrate the BER performance versus Threshold in the case of two fixed Rs values. We can observe that the constellation A is well edge detected, while the constellation B has a lot of redundant data. It can be seen from the aforementioned experimental results that the edge detection algorithm can achieve comparatively optimal performance when the threshold is 0.072 and Rs is 0.2, the parameters adopted in rear experiments.
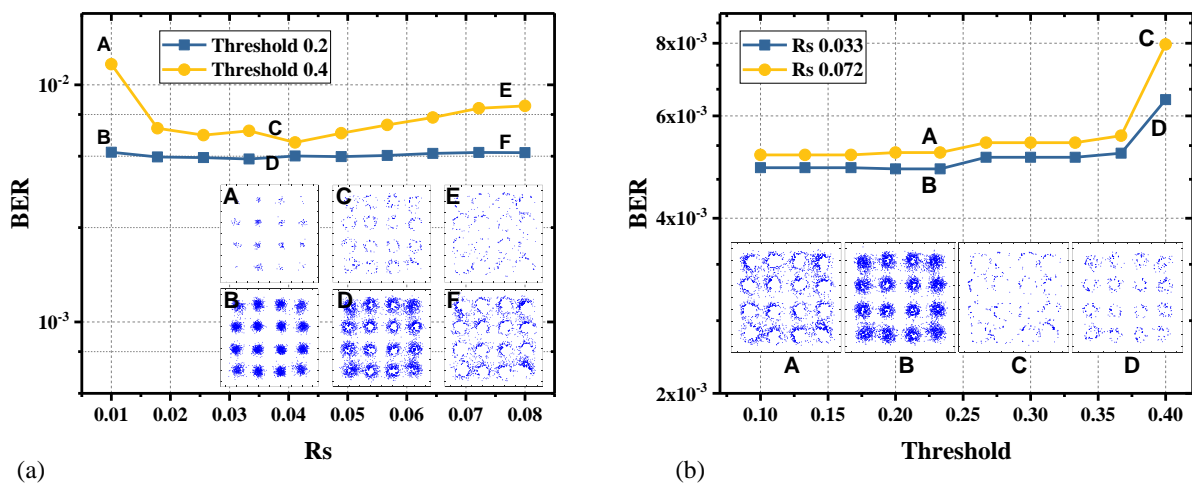
Figure 6. (**a**) BER versus the pixel-division size Rs and (**b**) BER versus the Sobel parameter Threshold at 1.6 Gbps.

Next, we investigate the BER versus box constraint, which is a key parameter of SVM, corresponding to *C* in Equation (2). The BER performance is measured by changing box constraint from 0.1 to 100 at 1.4 Gbps and 1.6 Gbps. As shown in Figure 7, when the box constraint increases, the BER firstly decreases. When the box constraint reaches around 1, the BER drops to a minimum value, and the BER gradually increases as the box constraint increases. The constellation diagrams at 1.4 Gbps and 1.6 Gbps are inserted as inset (i) and inset (ii), respectively. The trend of the BER curve at 1.4 Gbps is slowly varying because the ISI is not severe at a low data rate, and the boundary of constellation clusters is clear. However, when the data rate exceeds 1.6 Gbps, the constellation is distorted more severely. BER increases significantly as box constraint becomes larger, indicating that it is more at risk of overfitting. When the box constraint is 1, the SVM-based soft decision performs well at the two data rates. We can infer that constellation with less distortion has higher tolerance for the variation of box constraint. The parameter can be obtained at the condition with a high data rate and applied to other operation condition with lower data rate.
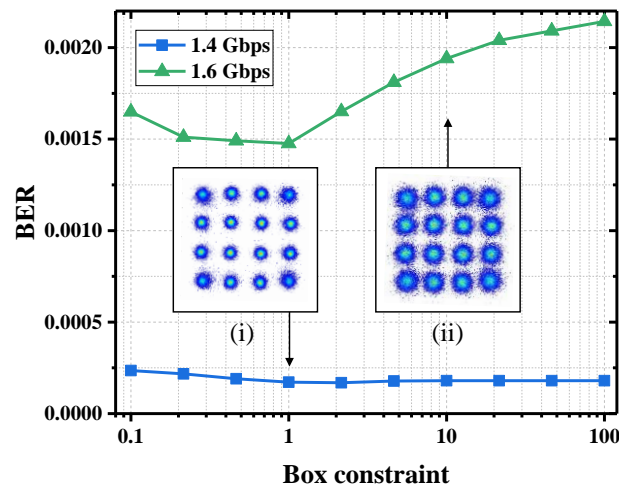
Figure 7. BER versus box constraint at 1.4 Gbps and 1.6 Gbps. (i) and (ii) are constellations at 1.4 Gbps and 1.6 Gbps respectively.

Figure 8 shows the projection of 4-D constellation points on a 2-D plane. The decision boundary obtained by SVM is also illustrated. Since the four axes are combined in pairs, six different projection planes can be illustrated (Figure 8a–f). As can be seen from Figure 8a,f, the constellation points spread out into a nearly circular shape because the axes of the projection plane are from the same time while the constellation clusters in Figure 8b–e spread out into an oval shape because the axes are from different time. The correlation between the two consecutive symbols will crosstalk each other and lead to the special ellipse constellation. Additionally, the outer constellation points spread more than the inner circle, which indicates the nonlinear effect in the UVLC system. The SVM-based decision boundary for elliptical constellation clusters is adjusted adaptively according to the distribution characteristics of constellation points. Therefore, the proposed method can deal with the distortion resulting from residual nonlinearity and ISI after post-equalization. The adaptive decision boundary is supposed to outperform the simple hard decision.
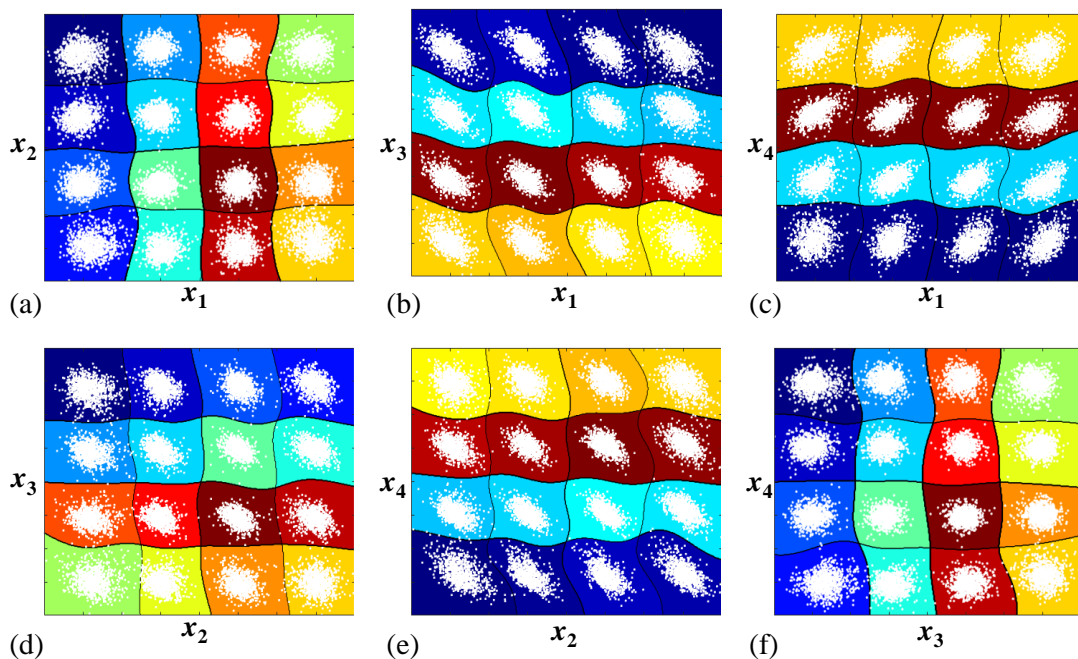

Figure 8. (**a**–**f**) are the projection of 4-D constellation points on a 2-D plane and the SVM-based soft decision boundary.

Figure 9 shows the BER performance on different baud rare under conditions without SVM, normal 2-D constellation with SVM (abbreviated as 2-D SVM in Figure 9), and 4-D constellation with SVM (abbreviated as 4-D SVM in Figure 9) after post-equalization. It should be noted that the SVM-based soft decision is applied in the decoding process, independent of the post-equalization. The solid lines are results employing LMS-based linear equalization. Obviously, 4-D constellation with SVM performs best, followed by normal 2-D constellation with SVM and without SVM. When the baud rate is low, the nonlinear effect is the dominant impairment, normal 2-D constellation with SVM can provide a significant performance gain. However, as the baud rate increases, ISI becomes the dominant impairment, 4-D constellation with SVM displays a larger performance gain. At the operating condition of 412.5 MBaud, the BER of LMS without SVM and LMS with 2-D SVM has exceeded the 7% FEC threshold (3.8×10^3), while the BER of LMS with 4-D SVM still satisfies the threshold. The available baud rate is increased by 12.5 MBaud, corresponding to the data rate improvement of 50 Mbps.
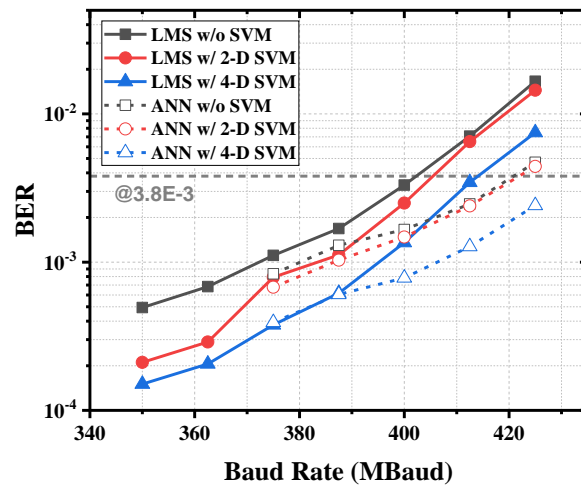

Figure 9. BER versus Baud rate with hard decision and SVM-based soft decision.

For fair comparison, we also add the results employing artificial neural network (ANN) for nonlinear equalization as the dashed lines in Figure 9. The ANN is a feedforward complex-valued network with a dual branch structure [6]. The input layer has 21 nodes, sharing the linear and nonlinear branches. The nonlinear branch contains one hidden layer with 10 nodes. The activation function is complex-ReLU. The Adam optimizer is used for training. We can observe that the ANN-based nonlinear equalization performs better than the LMS-based linear equalization. With the joint effort of 4-D SVM soft decision, the BER can keep under the threshold at 425 MBaud. It should be noted that the training size is 26,214, whereas after data preprocessing the training size is decreased by 56%. As the complexity of the training phase scales between $O(dN_t^2)$ and $O(dN_t^3)$ for SVM with d-dimensional feature vectors and N_t training points, the required computational resource has been significantly reduced.

5. Conclusions

In this paper, we propose to use SVM-based soft decision for consecutive-symbol-expanded 4-D constellation in bandwidth-limited nonlinear UVLC system. To reduce the computational complexity, bit-based binary SVM multi-class strategy and data preprocessing method are employed. Key parameters of the proposed method are discussed. Experimental results prove that the performance can be significantly improved. When LMS-based linear equalizer is used for post-equalization, the available baud rate is increased from 400 MBaud to 412.5 MBaud, corresponding to the data rate improvement of 50 Mbps. With the joint effort of nonlinear equalizer and the proposed scheme, the BER can still satisfy the 7% FEC threshold at 425 MBaud.

References

1. Hu, F.; Chen, S.; Li, G.; Zou, P.; Zhang, J.; Hu, J.; Zhang, J.; He, Z.; Yu, S.; Jiang, F.; et al. Si-Substrate LEDs with Multiple Superlattice Interlayers for beyond 24 Gbps Visible Light Communication. *Photonics Res.* **2021**, *9*, 1581. [CrossRef]
2. Duntley, S.Q. Light in the Sea*. *J. Opt. Soc. Am.* **1963**, *53*, 214. [CrossRef]
3. Elamassie, M.; Miramirkhani, F.; Uysal, M. Performance Characterization of Underwater Visible Light Communication. *IEEE Trans. Commun.* **2019**, *67*, 543–552. [CrossRef]
4. Jamali, M.V.; Nabavi, P.; Salehi, J.A. MIMO Underwater Visible Light Communications: Comprehensive Channel Study, Performance Analysis, and Multiple-Symbol Detection. *IEEE Trans. Veh. Technol.* **2018**, *67*, 8223–8237. [CrossRef]
5. Zhou, Y.; Zhu, X.; Hu, F.; Shi, J.; Wang, F.; Zou, P.; Liu, J.; Jiang, F.; Chi, N. Common-Anode LED on a Si Substrate for beyond 15 Gbit/s Underwater Visible Light Communication. *Photonics Res.* **2019**, *7*, 1019. [CrossRef]
6. Niu, W.; Chen, H.; Hu, F.; Shi, J.; Ha, Y.; Li, G.; He, Z.; Yu, S.; Chi, N. Neural-Network-Based Nonlinear Tomlinson-Harashima Precoding for Bandwidth-Limited Underwater Visible Light Communication. *J. Light. Technol.* **2022**, *40*, 2296–2306. [CrossRef]
7. Chi, N.; Zhao, Y.; Shi, M.; Zou, P.; Lu, X. Gaussian Kernel-Aided Deep Neural Network Equalizer Utilized in Underwater PAM8 Visible Light Communication System. *Opt. Express* **2018**, *26*, 26700. [CrossRef]
8. Jiang, H.; Qiu, H.; He, N.; Popoola, W.; Ahmad, Z.; Rajbhandari, S. Performance of Spatial Diversity DCO-OFDM in a Weak Turbulence Underwater Visible Light Communication Channel. *J. Light. Technol.* **2020**, *38*, 2271–2277. [CrossRef]
9. Zhou, Y.; Wei, Y.; Hu, F.; Hu, J.; Zhao, Y.; Zhang, J.; Jiang, F.; Chi, N. Comparison of Nonlinear Equalizers for High-Speed Visible Light Communication Utilizing Silicon Substrate Phosphorescent White LED. *Opt. Express* **2020**, *28*, 2302. [CrossRef]
10. Hu, F.; Lerma, J.A.H.; Mao, Y.; Zou, P.; Shen, C.; Ng, T.K.; Ooi, B.S.; Chi, N. Demonstration of a Low-Complexity Memory-Polynomial-Aided Neural Network Equalizer for CAP Visible-Light Communication with Superluminescent Diode. *Opto-Electron. Adv.* **2020**, *3*, 200009. [CrossRef]
11. Chi, N.; Zhou, Y.; Wei, Y.; Hu, F. Visible Light Communication in 6G: Advances, Challenges, and Prospects. *IEEE Veh. Technol. Mag.* **2020**, *15*, 93–102. [CrossRef]
12. Niu, W.; Ha, Y.; Chi, N. Support Vector Machine Based Machine Learning Method for GS 8QAM Constellation Classification in Seamless Integrated Fiber and Visible Light Communication System. *Sci. China Inf. Sci.* **2020**, *63*, 1–12. [CrossRef]
13. Wang, C.; Du, J.; Chen, G.; Wang, H.; Sun, L.; Xu, K.; Liu, B.; He, Z. QAM Classification Methods by SVM Machine Learning for Improved Optical Interconnection. *Opt. Commun.* **2019**, *444*, 1–8. [CrossRef]
14. Wang, D.; Zhang, M.; Li, Z.; Cui, Y.; Huang, S.; Wang, H. Optimized SVM-Based Decision Processor for 16QAM Coherent Optical Systems to Mitigate NLPN. In Proceedings of the Asia Communications and Photonics Conference 2015, Hong Kong, China, 19–23 November 2015; 2015; 1, pp. 4–6. [CrossRef]
15. Cui, Y.; Zhang, M.; Wang, D.; Liu, S.; Li, Z.; Chang, G.-K. Bit-Based Support Vector Machine Nonlinear Detector for Millimeter-Wave Radio-over-Fiber Mobile Fronthaul Systems. *Opt. Express* **2017**, *25*, 26186. [CrossRef]
16. Zhang, J.; Chen, W.; Gao, M.; Shen, G. K-Means-Clustering-Based Fiber Nonlinearity Equalization Techniques for 64-QAM Coherent Optical Communication System. *Opt. Express* **2017**, *25*, 27570. [CrossRef] [PubMed]
17. Wu, X.; Chi, N. The phase estimation of geometric shaping 8-QAM modulations based on K-means clustering in underwater visible light communication. *Opt. Commun.* **2019**, *444*, 147–153. [CrossRef]
18. Lu, F.; Peng, P.C.; Liu, S.; Xu, M.; Shen, S.; Chang, G.K. Integration of Multivariate Gaussian Mixture Model for Enhanced PAM-4 Decoding Employing Basis Expansion. In Proceedings of the Optical Fiber Communication Conference 2018, San Diego, CA, USA, 11–15 March 2018; Volume 2, pp. 1–3.
19. Wu, X.; Hu, F.; Zou, P.; Chi, N. Application of Gaussian Mixture Model to Solve Inter-Symbol Interference in PAM8 Underwater Visible Light System Communication. *IEEE Photonics J.* **2019**, *11*, 7907810. [CrossRef]

20. Chi, N.; Liang, S. Enabling Technologies for High-Speed Visible Light Communication Employing CAP Modulation. *J. Light. Technol.* **2018**, *36*, 510–518. [CrossRef]
21. Haigh, P.A.; Chvojka, P.; Ghassemlooy, Z.; Zvanovec, S.; Darwazeh, I. Visible Light Communications: Multi-Band Super-Nyquist CAP Modulation. *Opt. Express* **2019**, *27*, 8912. [CrossRef]
22. Zibar, D.; De Carvalho, L.H.H.; Piels, M.; Doberstein, A.; Diniz, J.; Nebendahl, B.; Franciscangelis, C.; Estaran, J.; Haisch, H.; Gonzalez, N.G.; et al. Application of Machine Learning Techniques for Amplitude and Phase Noise Characterization. *J. Light. Technol.* **2015**, *33*, 1333–1343. [CrossRef]
23. Burges, C.J.C. A Tutorial on Support Vector Machines for Pattern Recognition. *Data Min. Knowl. Discov.* **1998**, *2*, 121–167. [CrossRef]
24. Wu, X. Incorporating Prior Knowledge with Weighted Margin Support Vector Machines. In Proceedings of the 10th ACM SIGKDD International Conference on Knowledge Discovery and Data Mining, Seattle, WA, USA, 22–25 August 2004; pp. 326–333.
25. Zou, P.; Zhao, Y.; Hu, F.; Chi, N. Underwater Visible Light Communication at 3.24 Gb/s Using Novel Two-Dimensional Bit Allocation. *Opt. Express* **2020**, *28*, 11319. [CrossRef] [PubMed]